ABSTRACT

Ray-tracing Techniques and The Simulation of Large-Scale In-Flight Wi-Fi Signal Propagation

Riley D. DeHaan

Director: Yang Li, Ph.D.

As consumer expectations for data usage continue to rise, the acceptance of poor connectivity on airplanes will become increasingly untenable. Reliable, high speed in-flight connectivity is in high demand in the airline industry. One challenge associated with designing in-flight wireless networks is understanding how electromagnetic waves propagate within the airplane cabin. In this thesis, a passenger airplane is modeled using FEKO electromagnetic simulation software, and ray-tracing simulations of Wi-Fi signal propagation throughout the plane are conducted. Large-scale fading parameters of the path loss factor and the standard deviation of shadowing are extracted from the simulation results and compared to those of field tests performed by other authors. The modeling results show good agreement with those of other authors and of theoretical predictions and demonstrate the potential of using ray-tracing techniques for modeling wireless propagation in aircraft cabins.

APPROVED BY DIRECTOR OF HONORS THESIS:

_____

Dr. Yang Li, Department of Electrical and Computer Engineering

APPROVED BY THE HONORS PROGRAM

_____

Dr. Elizabeth Corey, Director

DATE: _____

RAY-TRACING TECHNIQUES AND THE SIMULATION OF LARGE-SCALE IN-FLIGHT WI-FI SIGNAL PROPAGATION

A Thesis Submitted to the Faculty of

Baylor University

In Partial Fulfillment of the Requirements for the

Honors Program

By

Riley DeHaan

Waco, Texas

May 2018

TABLE OF CONTENTS

ACKNOWLEDGMENTS

I would like to thank my friends at Baylor and my family for supporting me throughout my undergraduate experience and Dr. Li for his incredible guidance and patience throughout the process of my writing this thesis.

CHAPTER ONE

Introduction

In recent years, electronic connectivity for accessing data and for communications has changed from a luxury to an expectation as its role in work, communication, and entertainment has continued to rapidly expand. Communications companies have strained to satisfy the growing consumer demand for ubiquitous and unlimited connectivity by building extensive networks of towers, cables, satellites, and routers which currently provide access to countless electronic devices. One of the last frontiers however to which data connectivity and remote communications have not yet been extended consistently and inexpensively is the airplane cabin, which represents a unique challenge for connectivity. First the location of flight is far above the coverage of terrestrial networks and planes flying at high speeds and often through multiple nations (with differing communication regulations and band allocations) must typically be connected to the terrestrial network through satellites which often have lower connection speeds than ground networks, at least with current protocols [1, 2]. Secondly, even with a connection to the ground network, it is difficult to connect users within the cabin environment itself. Adding more wired data connections is generally undesirable given the severe limits on weight and space for cable bundles with cables increasing plane fuel costs, design costs, and manufacturing costs [3].

Airlines are then strongly motivated to develop wireless communications to service passengers and to reduce existing aircraft cabling used for communication

between cabin crew members and for aircraft sensor communication [4]. However, the aircraft cabin also poses problems for wireless connectivity. Relative to the indoor propagation environments in buildings which have been studied extensively, airplane cabins have a high density of signal attenuating clutter, a large number of users which both block signals and must be serviced in a condensed cylindrical space, and a metallic, reflective tunnel-like fuselage structure leading to waveguide effects, signal distortion, and multipath [4, 5]. Some of these factors, such as increased clutter tend to increase signal attenuation while other factors, such as the waveguide effects of the fuselage structure tend to decrease attenuation, making for a complex propagation environment. Nonetheless airlines are making progress with a growing multibillion dollar communications market at stake [1].

To improve signal coverage, accurate modeling of the wireless propagation in the aircraft fuselage is needed. In free space, the power received by a receiver from a transmitter is described by the Friis free space equation:

$$P_R(d) = P_T G_T G_R \lambda^2 / ((4\pi)^2 d^2 L) \quad (1)$$

where P_R gives the received power, P_T the transmitted power, d the distance between transmitter and receiver, G_T and G_R the transmitter and receiver antenna gains respectively, L the system loss factor, and λ the signal wavelength [6]. From the Friis free space equation, signal power can be seen to decrease in free space with the inverse square of the separation distance between receiver and transmitter. The dependence of signal strength on transmitter-receiver separation is an important relation for determining the radio coverage of a given area. For environments other than free space, this dependence

is also commonly described by an inverse power law, but with an exponent reflecting the rate of attenuation particular to that environment. Written in decibel scale, the path loss model gives the path loss or attenuation with distance:

$$PL(d)[dB] = \overline{PL}(d_o)[dB] + 10\, n \log(d/d_o) + \chi_\sigma \quad (2)$$

where d again gives the TX-RX separation distance, d_o gives a reference distance (typically one meter), n gives the path loss exponent or path loss factor (which for free space has a value of two by the Friis free space equation) describing the rate of signal attenuation, and χ_σ is a log-normally distributed zero mean random variable with standard deviation σ [6]. χ_σ describes shadowing effects due to randomly varying levels of clutter for different receiver locations with equal separation distance from the transmitter [6]. The first term $\overline{PL}(d_o)$ gives a reference path loss at the reference distance. This reference path loss empirically incorporates the effects of all of the factors contained in the Friis free space equation other than distance and the path loss factor. The received power P_R as a function of transmitted power P_T and path loss PL is given by

$$P_R(d)[dBm] = P_T[dBm] - PL(d)[dB] \quad (3)$$

The path loss model describes the large-scale fading characteristics or the degree and variability of signal attenuation over TX-RX separation distances on the order of at least several wavelengths in a particular environment and does not directly account for small-scale fading or the more rapid variation over sub-wavelength scales in signal strength due to multipath interference [6]. The estimate of attenuation which the model provides is useful for predicting signal strength. The signal strength at a given location is a significant determiner of data bit error rates at that location with stronger signal

strengths, or equivalently, higher signal-to-noise ratios (SNR), intuitively yielding generally lower bit error rates in transmission since the effect of random noise in distorting the information signal is lower. Higher bit error rates in turn imply lower bit rates or connection speeds and smaller areas of signal coverage [7]. The parameter χ_σ describing (large-scale) shadowing effects gives a margin of statistical fade depth by which a signal must be boosted to ensure coverage in an area exhibiting shadowing effects [3]. The path loss model is then useful in the design of radiocommunications systems and has been studied extensively for various environments including commercial passenger cabins with simulations and measurements.

In [3], the path loss factors at 2.45 GHz (the frequency of WiFi signals) on a Bombardier CRJ700, a smaller commercial plane with 70 passenger seats, for line-of-sight (LOS) measurements were found to be between 1.3 (for measurements taken along the cabin aisle) and 2 (for measurements taken along the cabin seats). The LOS shadowing standard deviations were found to be between 5.4 dB (along the aisle) and 7.5 dB (along the seats). For non-line-of-sight (NLOS) measurement scenarios, path loss factors of 2.2 and 2.7, both for measurements along the seats of the cabin, were reported with shadowing standard deviations of 8 dB and 9.8 dB. Thus for LOS link scenarios, this cabin was found to likely exhibit waveguide effects with path loss factors or rates of attenuation with distance below or equal to that of the factor of two in free space. NLOS measurement scenarios as expected yielded higher rates of attenuation, in this case greater than that of free space. Higher variability due to shadowing was also seen for the

NLOS scenarios relative to the LOS scenarios as would also be expected given the higher average level of obstruction inherent to NLOS scenarios.

The authors of [5] computed path loss factors with power measurements taken on an Airbus 321, a midsize commercial plane, for a band from 1805 MHz to 1880 MHZ and found the path loss factors of the environment to increase with TX-RX distance and to depend on the direction of propagation from TX to RX, whether toward the front of the airplane (the "in-flight" direction) or toward the back (the "in-rear" direction). In the in-rear direction, path loss factors of 1.5, 2, and 2.6 were measured for TX-RX distance ranges of 1 meter to 5 meters, 5 meters to 14 meters, and greater than 14 meters respectively. In the in-flight direction, path loss factors of 1.5, 2.3, and 2.6 were measured for TX-RX distance ranges of 1 meter to 5 meters, 5 meters to 14 meters, and greater than 14 meters respectively. The increase in path loss factor with TX-RX distance is attributed to the decrease in the directness of the link between the receiver and transmitter with receivers close to the transmitter having a nearly LOS link with the transmitter due to the strong reflections off the chairs close to the transmitter and the receiver. As TX-RX distance increases, the significance of this reflection decreases, leading to increased rates of attenuation. The difference between the path loss factors between the in-rear and in-flight propagation directions is attributed to differences between the chair materials in the fronts and backs of the cabin seats.

In [4], path loss factors were estimated with power measurements from a Boeing 737-200, another commercial plane, over a band from 3 GHz to 10.6 GHz for wideband applications. The receiver location was varied in these measurements between positions

throughout the cabin at the headrests, armrests, and footrests of numerous seats. Additionally, the level to which the cabin was filled with seated passengers was also varied from being empty, to being half filled, to being fully filled. For the scenarios with an empty plane cabin, path loss factors between 2.1 and 2.2 were obtained. For scenarios with a half filled cabin, path loss factors between 1.9 and 2.5 were measured. For the scenarios with a completely filled cabin, path loss factors between 1.7 and 2.6 were measured. The results show an increase in path loss factor with increasing degree of passenger loading as would be expected given passenger bodies tend to increase the level of signal-blocking clutter in the cabin. The lower end of the ranges of path loss factors decrease with increasing passenger seating and interestingly the lower end of the ranges always correspond to the footrest receiver positions. The armrest and headrest positions always showed increasing path loss factor with increasing passenger seating. However, the footrest positions have the highest reference path loss of the three receiver seat positions and the highest overall path loss of the three positions as expected given the greater obstruction between the transmitter positions and the footrest receiver positions. The degree of passenger seating is a parameter of the propagation environment examined in our work and it is expected our simulations will predict larger path loss factors for greater passenger seating levels.

In [7], path loss factors of 2.0122 and 2.2851 were found for LOS and NLOS scenarios respectively at 3.423 GHz in an empty plane cabin. Here again decreased rates of attenuation are seen for lower levels of obstruction of the signal and these results for an empty cabin closely match those reported in [4] for an empty cabin. On the lower end

of the spectrum of path loss factor values, the results of [8] show path loss factors ranging between 0.20 and 2.08 with the majority of measurement scenarios resulting in path loss factors below 1.5 in a C-130 Hercules military plane having significantly more metallic surfaces than typically found in commercial passenger planes. As expected, the highly reflective metallic surfaces lead to lower attenuation in this environment compared to typical cabins of commercial aircraft which have more plastic and textile surfaces to partially absorb and dissipate the RF energy of waves impinging on these dielectric materials [6].

The path loss model has additionally been studied for propagation environments outside of airplanes in buildings and over terrestrial environments. While these results are not as applicable to verifying the results of simulations of propagation in airplane cabins, which as mentioned have propagation characteristics different from those of common indoor propagation environments, some indoor environments such as hallways are similar in structure to the tunnel-like form of an airplane fuselage and empirical path loss factor estimates for these structures can be useful for comparison with our simulation results. In [9], the path loss factors in a hallway of the BRIC, a Baylor research facility, were measured over a band from 2 GHz to 3 GHz. At 2.45 GHz, a low path loss factor 1.42 was obtained with a standard deviation of shadowing of 5.1 dB. Table I gives a summary of the path loss model parameters referenced.

While measurement campaigns are a necessary part of validating RF system performance, computer simulations of signal propagation are often used to provide reasonable assurance of performance prior to implementation. Simulations reduce the

TABLE I
Summary of Measured Path Loss Model Parameters

Reference	Plane	Frequency (GHz)	Scenario Description	LOS/ NLOS	TX height (m)	RX Height (m)	RX along Seats/Aisle	Reference Power at 1 m (dBm)	PL(1 m) (dB)	n	σ (dB)
[3]	Bombardier CRJ700	2.45	-	NLOS	1.2	0.5	Seats	-	26	2.7	9.8
[3]	Bombardier CRJ700	2.45	-	LOS	1.2	1	Seats	-	28.1	2	7.3
[3]	Bombardier CRJ700	2.45	-	NLOS	1.6	0.5	Seats	-	29.83	2.2	8
[3]	Bombardier CRJ700	2.45	-	LOS	1.6	1	Seats	-	28.4	2	7.5
[3]	Bombardier CRJ700	2.45	-	LOS	1.6	0.5	Aisle	-	28	1.3	5.4
[3]	Bombardier CRJ700	2.45	-	LOS	1.6	1	Aisle	-	27.26	1.6	6.4
[5]	Airbus A321	1.805-1.88	1m-5m, in-rear direction	NLOS	2.49	0.75	Seats	-	-	1.5	2.55
[5]	Airbus A321	1.805-1.88	5m-14m, in-rear direction	NLOS	2.49	0.75	Seats	-	-	2	1.84
[5]	Airbus A321	1.805-1.88	14m+, in-rear direction	NLOS	2.49	0.75	Seats	-	-	2.6	3.01
[5]	Airbus A321	1.805-1.88	1m-5m, in-flight direction	NLOS	2.49	0.75	Seats	-	-	1.5	1.81
[5]	Airbus A321	1.805-1.88	5m-14m, in-flight direction	NLOS	2.49	0.75	Seats	-	-	2.3	2.49
[5]	Airbus A321	1.805-1.88	14m+, in-flight direction	NLOS	2.49	0.75	Seats	-	-	2.6	3.39
[4]	Boeing 737-200	3-10.6	Empty	NLOS	2.2	Headrest	Seats	-40	-	2.1	5
[4]	Boeing 737-200	3-10.6	Empty	NLOS	2.2	Armrest	Seats	-42.6	-	2.2	5.1
[4]	Boeing 737-200	3-10.6	Empty	NLOS	2.2	Footrest	Seats	-45.1	-	2.2	4.7
[4]	Boeing 737-200	3-10.6	Half filled	NLOS	2.2	Headrest	Seats	-39.7	-	2.4	5.3
[4]	Boeing 737-200	3-10.6	Half filled	NLOS	2.2	Armrest	Seats	-43.1	-	2.5	5.2
[4]	Boeing 737-200	3-10.6	Half filled	NLOS	2.2	Footrest	Seats	-49.1	-	1.9	3.8
[4]	Boeing 737-200	3-10.6	Filled	NLOS	2.2	Headrest	Seats	-39.9	-	2.6	4
[4]	Boeing 737-200	3-10.6	Filled	NLOS	2.2	Armrest	Seats	-46	-	2.5	3.9
[4]	Boeing 737-200	3-10.6	Filled	NLOS	2.2	Footrest	Seats	-50.9	-	1.7	2.4
[7]	Commercial Plane	3.423	-	LOS	-	-	-	-	-	2.0122	-
[7]	Commercial Plane	3.423	-	NLOS	-	-	-	-	-	2.2851	-
[8]	Hercules C-130	3.1-10.6	Metallic plane	LOS	1.35	1.35	Aisle	-	28.06	0.9	0.45
[8]	Hercules C-130	3.1-10.6	Metallic plane	LOS	2.5	0.7	Seats	-	34.73	0.66	0.63
[9]	BRIC Hallway	2-3	-	LOS	0.95	0.95	-	-	-	1.7	5.13
[9]	BRIC Hallway	2.45	-	LOS	0.95	0.95	-	-	42.55	1.42	5.1

need for expensive measurements of signal strength (which are usually valid only for the plane model the measurements are taken on) and decrease the likelihood of needing to retrofit a plane after manufacturing. A wide variety of simulation methods exist for computing numerical solutions to Maxwell's equations. Many of these methods however are computationally impractical for electrically large structures, such as those the size of airplanes at 2.45 GHz [10]. Instead, RF designers have turned to approximate or asymptotic solutions to Maxwell's equations such as ray-tracing techniques in simulating signal propagation in larger structures [10]. In particular, ray-tracing methods have been used by several authors to accurately predict characteristics of signal propagation in the UHF band. In [11], ray-tracing simulations predicted signal powers in close agreement to measured results in various locations throughout a Dassault Aviation Falcon business jet with all differences between simulation and measurement being below 4.5 dB. Ray-tracing methods have also been used to accurately predict RMS delay spread, a central measure of the arrival delays of signal reflections relative to the first received signal path component, along urban streets [12].

The fundamental concepts behind ray-tracing methods are easily visualized and were in fact developed originally in the field of optics [11]. Rays which locally represent a wavefront and point in the direction of local macroscopic flow of RF energy of the wavefront are typically launched from a point source and traced in their respective ray directions [11, 13]. If a ray encounters a smooth boundary between the incident propagation medium and a propagation medium with electrical and magnetic properties different from those of the incident medium, the ray will be partially reflected back into

the incident medium and partially transmitted into the medium impinged upon, generating a reflected ray and a transmitted ray [6] (see Figure 1). The direction of the reflected ray may be calculated using the Law of Reflection, which states that the angle of incidence equals the angle of reflection (relative to the boundary normal vector) [6]. The direction of the transmitted ray can be determined with Snell's Law, which accounts for the material properties of the incident and impinged media [6]. Intuitively, as the number of rays modeling a wavefront approaches infinity, each ray will provide an increasingly accurate local approximation of the wavefront and the set of all rays will converge to a perfect representation of the surface of the overall wavefront**.** Additionally, as the number of ray interactions, such as reflections and transmissions of rays, is increased, the more accurately the rays will model the phenomena of reflection and transmission of real wavefronts. Practically, the number of ray interactions must be limited in real simulations to allow for finite computation times. This limitation often does not significantly affect the simulation accuracy because after several ray interactions, the signal power associated with a ray is negligible.

Signal propagation is also affected by scattering, the effect of rough surfaces reflecting signals in many directions or "scattering" signals, and by diffraction, which is a phenomenon in which waves bend behind obstacles [6]. The theory of geometric optics does not account for the effects of scattering and diffraction. However the Geometric Theory of Diffraction (GTD) has been developed to account for the effects of diffraction in ray-tracing [12] and scattering models depending on the Rayleigh criterion of roughness have been used to include scattering effects in ray-tracing methods [10].

Ray-tracing methods are based on the theory of Geometric Optics (GO), which models electromagnetic (EM) waves as collections of rays traveling in the direction of wave propagation. GO may be accurately applied if the wavelength of the propagating wave is significantly smaller than the dimensions of the propagation environment. For WiFi signals at 2.45 GHz, the wavelength in free space is approximately 12.2 cm, far smaller than the dimensions of airplanes and thus the GO approximation is reasonable for modeling WiFi signal propagation in plane cabins [10].

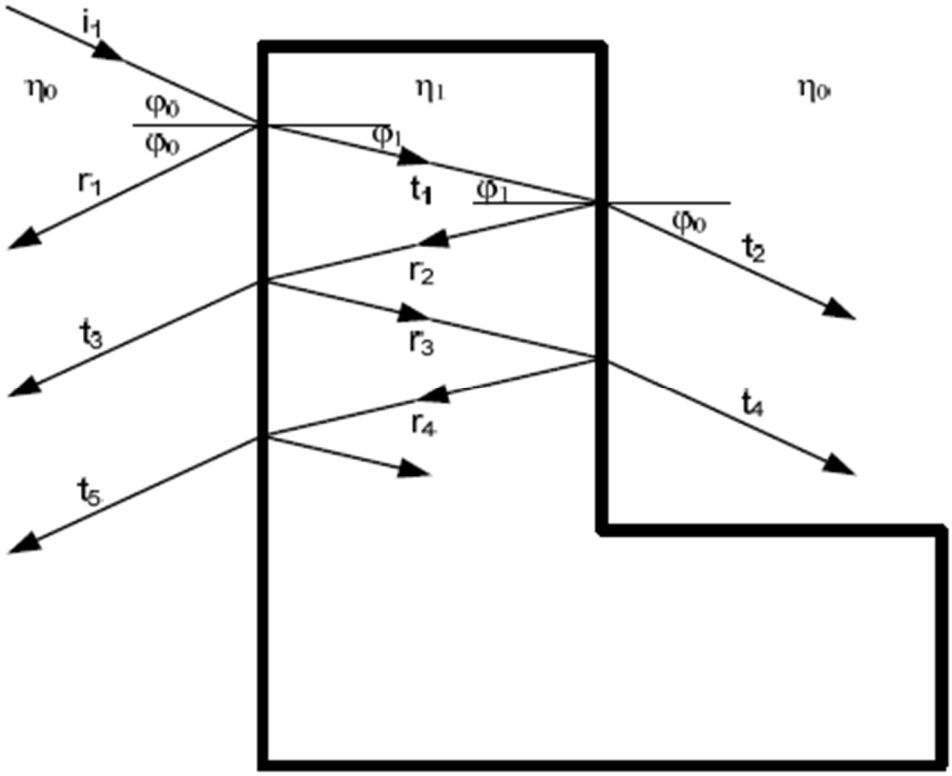

Fig. 1. Reflection and transmission of an incident wavefront (represented by a ray i_1 traveling perpendicularly to the wave front) propagating in a medium with index of refraction η_0 impinging on a medium with index of refraction η_1. The reflected ray r_1 travels at an angle relative to the boundary normal equal to the angle of the incident ray relative to the normal. The path of the transmitted ray t_1 is "bent" slightly toward the normal in this case, indicating the index of refraction impinged upon is greater than the incident index of refraction by Snell's Law. The additional rays shown (r_2, t_2 r_3, etc.) are generated from the transmitted ray continuing to impinge upon boundaries of the two mediums. Image given in [10].

In this paper, a ray-tracing algorithm is used to model signal propagation in airplanes. Specifically the algorithm is used to predict path loss factors and standard deviations of shadowing in simplified, generic model plane environments. These predicted path loss parameters are compared with those obtained by the other mentioned authors from measurements of RF signals in planes similar to our model. The results of the simulations match the empirical results of these authors reasonably well and show promise for the use of ray-tracing in modeling the large-scale propagation characteristics of aircraft WiFi signals. In the remainder of this work, a description of the methods used in these simulations will be given followed by a presentation of the simulation results and the predicted path loss model parameters. Finally, the conclusions of these results will be discussed.

CHAPTER TWO

Methods

Simulations were performed on a simplified plane model which was intended to generally capture the predominant structural features of commercial airplanes of highly reflective metallic fuselage shells, potentially wave-guiding tunnel-like cabins, and periodic obstructions of lossy chairs and passengers, rather than to model any plane in particular. The model consists of a perfectly electrically conductive (PEC) fuselage shell enclosing a cabin area consisting of a floor and a ceiling between which are rows of chair structures (see Fig. 2). The chairs are organized into thirty rows of three chairs grouped into three sets and in some of the simulations, these chairs are populated with simple passenger bodies shown in Fig. 3. The fuselage shell has a length of 57 m, a height of about 6 m, and a width of about 5.9 m and is modeled after that of a Boeing 787-8, a commercial jet with a capacity of 242 passengers. The cabin floor extends from the front of the plane to the back with a length of 37.7 m and the height of the cabin ceiling above the cabin floor is about 2.5 m. The chairs have a height of 1.14 m above the cabin floor and the passengers each have a sitting height of 1.37 m above the cabin floor and a body width of 0.56 m. The x-axis of the model coordinate system is directed laterally from one side of the fuselage to the other, the y-axis is directed from the front (or nose) to the back (or tail) of the plane, and the z-axis gives elevation. The origin of the coordinate system is at the tip of the nose of the plane as may be seen in Fig. 2.

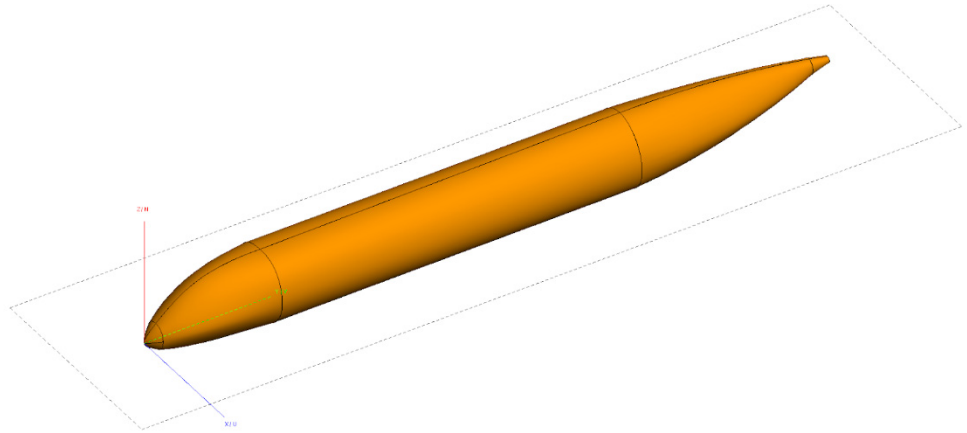

(a)

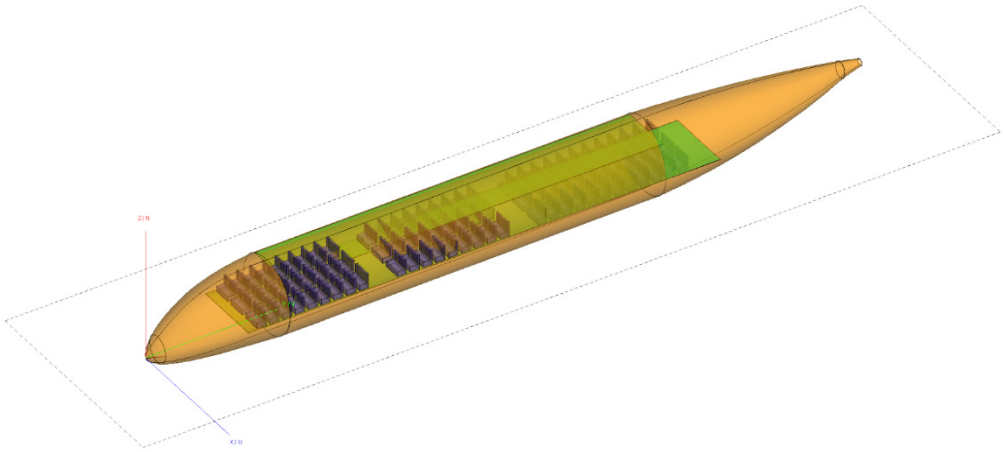

(b)

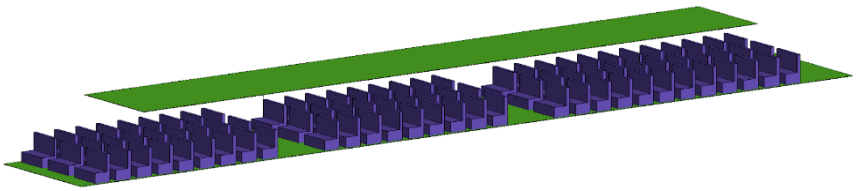

(c)

Fig. 2. The simulated CAD model of a commercial airplane. (a) The outer metallic fuselage shell of the model. (b) The model with transparent features to allow for a view of the internal structure of the cabin. (c) The cabin furnishings of three groups of rows of three chairs between a ceiling and a floor.

The transmitting antenna of the RF system of the plane was chosen to be a half-wave dipole for its simplicity and for generality of the simulation results. This transmitter was placed between the first set and second set of chairs along the centerline of the plane (in the YZ-plane) as shown in Fig. 3(b) and was excited by a voltage source with a magnitude of 1 V and a port impedance of 50 Ohms. The Poynting vector magnitude of the signal generated by this transmitter is computed along the model cabin on a horizontal planar surface at the elevation of the lower back level of the chairs where users would likely be using handheld devices in their lap, 0.64 meters above the cabin floor (see Fig. 3(c) below). This planar surface will be referred to as the receiver plane. In the receiver plane, propagated field values were computed at points arranged in a rectangular grid of equally spaced points with the grid having 401 points in the y-coordinate direction (along the length of the fuselage) and 61 points in the x-direction direction (along the width of the fuselage). The chairs, bodies, floor, and ceiling are modeled as lossy dielectrics with relative permittivities and loss tangents given in Table II.

TABLE II
Plane Model Electrical Material Properties

Material	Relative Permittivity	Loss Tangent
Chair (Leather)	1.4336	0.1339
Passenger (Body)	40.3975	0.2376
Ceiling/Floor	3.9996	0.0200
Fuselage Shell (PEC)	-	0

The simulations were run with the FEKO Ray-Launching-Geometric Optics (RL-GO) algorithm for a signal frequency of 2.45 GHz, the frequency of Wi-Fi and Bluetooth. The Poynting vector magnitude, a measure of signal power propagating orthogonally

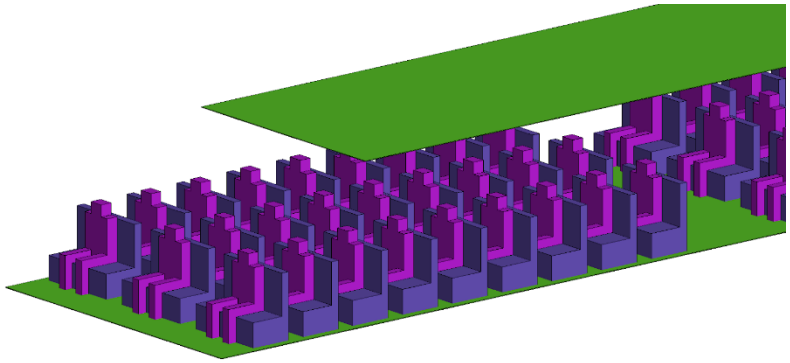

(a)

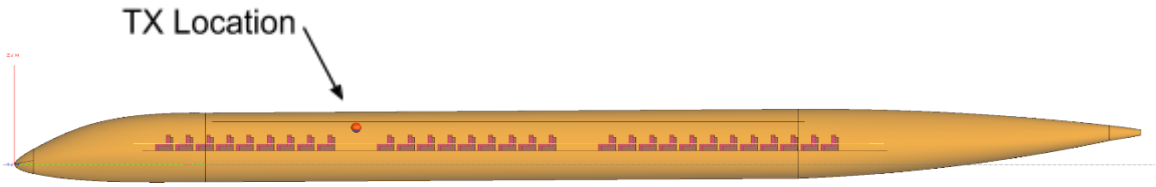

(b)

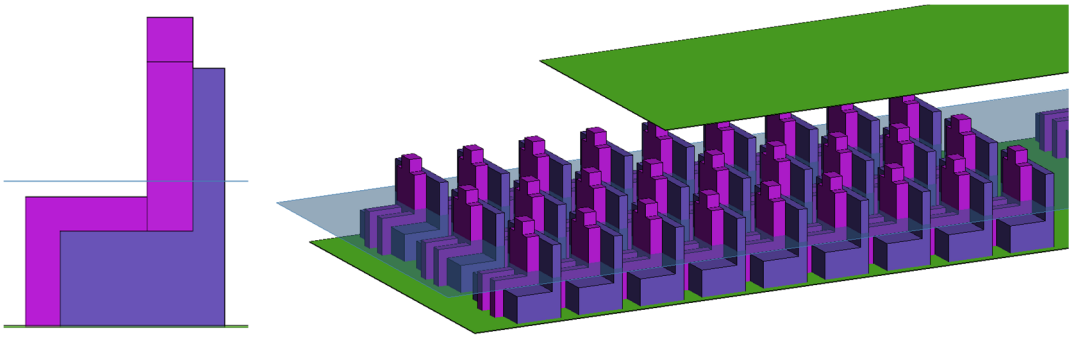

(c)

Fig. 3. (a) The cabin seated with passenger bodies. (b) The transmitter location within the cabin shown as the red dot positioned between the two front most sets of seats. (c) The receiver plane on which the Poynting vector magnitudes are computed shown as a blue planar surface at the elevation of the lower seatback.

through a unit area, was computed in the receiver plane with the electric field values calculated by a FEKO simulation near field request. The time-averaged Poynting vector magnitude $<S>$ as a function of the electric field strength $|E|$ is given by

$$<S> = \frac{1}{2} |E|^2/\eta \quad (4)$$

where η is the characteristic impedance of the medium of propagation taken for our computations to be free space as receiver antennas of consumer electronic devices are typically operated in air. Regressions of the Poynting vector magnitudes in decibel scale with respect to logarithmic TX-RX distance were taken along nine paths shown in Fig. 4 in the receiver plane running along the length of the plane.

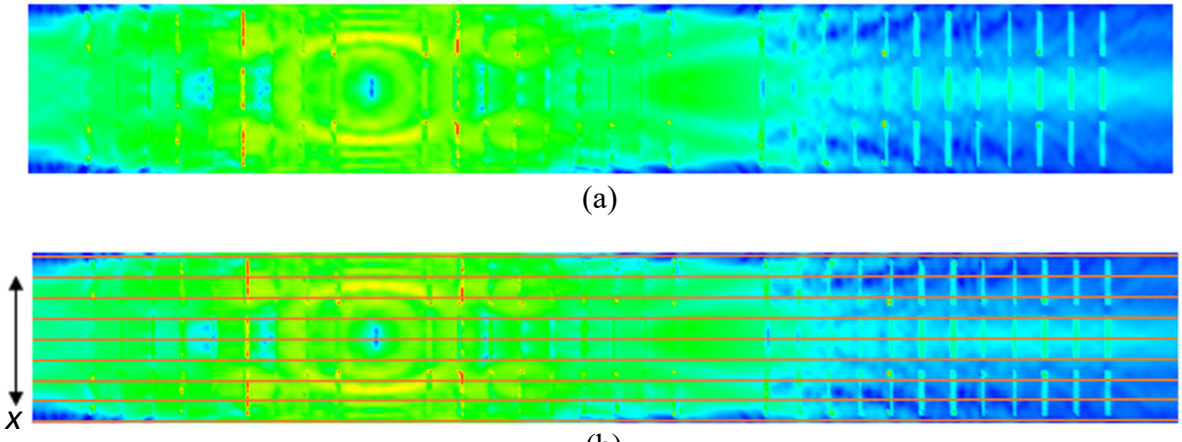

Fig. 4. (a) Typical color plot of the simulated Poynting vector magnitudes. (b) Same color plot with nine orange lines superimposed on top of the original plot to indicate the nine paths through the cabins of the linear regressions of decibel-scale Poynting vector magnitude versus logarithmic TX-RX separation distance.

These regressions of the Poynting vector magnitude estimate the path loss factor and standard deviation of shadowing for the model resulting from inserting (2) into (3), which essentially rewrites the path loss model discussed above in terms of power rather than in terms of attenuation:

$$P_R(d)[dBm] = \overline{P_R}(d_o)[dBm] - 10\, n \log(d/d_O) - \boldsymbol{\chi_\sigma} \quad (5)$$

where P_R again is the received signal power, $\overline{P_R}$ is the mean received signal power, d gives the TX-RX separation distance, d_O gives a reference distance (1 m for our computations), n gives the path loss factor, and $\boldsymbol{\chi_\sigma}$ is a log-normally distributed zero mean random variable describing shadowing effects with standard deviation $\boldsymbol{\sigma}$. For a given receiver antenna with a fixed relative orientation, the received power is given by the surface integral of the Poynting vector over the effective surface of the receiving antenna and is proportional to the Poynting vector magnitude (assumed to be locally constant for small antennas) at a location:

$$P_R = \langle S \rangle \cdot A_{eff} \quad (6)$$

where $\langle S \rangle$ is the time-averaged magnitude of the Poynting vector and A_{eff} is the effective aperture area of the receiving antenna for a given antenna orientation relative to the received fields [14]. The magnitude of the Poynting vector therefore provides a good estimate of the relative received signal strength at a particular location and may then be used to approximately predict the scaleless path loss parameters of path loss factor and standard deviation of shadowing as opposed to the received signal power at a given location which depends on the properties of a receiver antenna. These parameters are derived from linear least-squares regressions of the Poynting vector magnitude values in decibel scale computed from the FEKO RL-GO simulations versus logarithmic TX-RX separation distance along the regression paths shown in Fig. 4 (b).

The convergence and computational validity of the simulation results were confirmed with several convergence tests. The RL-GO algorithm launches rays from a

source with a user-specified ray-launching angular increment or angular increment between the paths of adjacently launched rays [15]. As discussed above, higher ray densities or equivalently, lower ray-launching degree increments, generally lead to more accurate simulations. The RL-GO algorithm also allows for specifying the number of ray interactions (reflections or transmissions) before a ray path is ended and as might be expected, simulation accuracy tends to increase with the number of ray interactions. For the simulations of this work, the ray-tracing angular increment was chosen to be 0.3 degrees (for both the phi and theta angular dimensions) and the number of ray-interactions was limited to three. These simulation settings were applied to all simulations used to compute the Poynting vector magnitudes from which path loss parameters were derived. The choice of ray-tracing angular increment was validated with convergence tests in which the angular increment was decreased from 0.7 degrees to 0.5 degrees to 0.3 degrees. Typical resulting plots of Poynting vector magnitude for these convergence tests are shown in Fig. 5.

During the process of simulating the signal propagation in the cabin, it was found that the degree of convergence and computation times of the simulations were improved significantly by using a fifth-scale model of the cabin. In the scaled-down model, the structural dimensions of the full-scale plane model were all reduced by a factor of five with the exception of the transmitting antenna, which was left unscaled. This scaling operation, as opposed to decreasing the signal frequency, decreases the electrical size of the model (thereby improving the convergence) while preserving the transmitter properties and the interaction of the plane media with the propagated signals at 2.45 GHz.

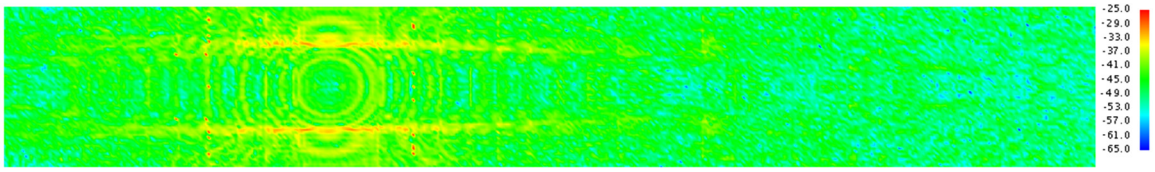

(a)

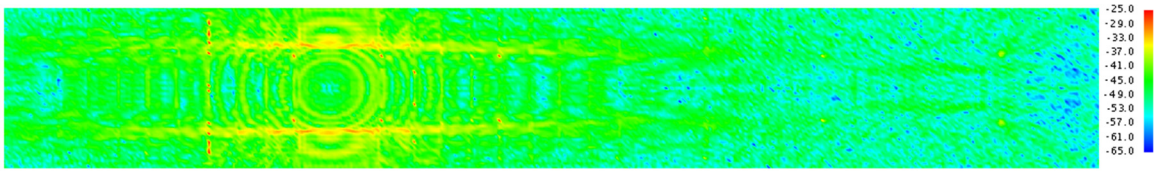

(b)

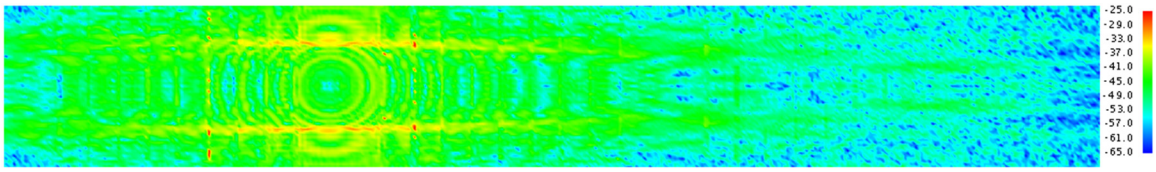

(c)

Fig. 5. Typical color plots of Poynting vector magnitude for full-scale model simulations demonstrating convergence of the simulations with ray-tracing angular increments of (a) 0.7 degrees, (b) 0.5 degrees, and (c) 0.3 degrees.

In personal correspondence with FEKO software representatives, this method of reducing the size of models was stated to have been used to good effect by other customers for electrically large models. Typical plots of Poynting vector magnitude of the convergence tests for the fifth-scale models are shown in Fig. 6. Qualitatively, the resulting values of the full-scale and fifth-scale models are in good agreement. There are two primary differences between the results of the full-scale and fifth-scale models shown in these convergence tests. First, the full-scale model plots show spottiness or high variability

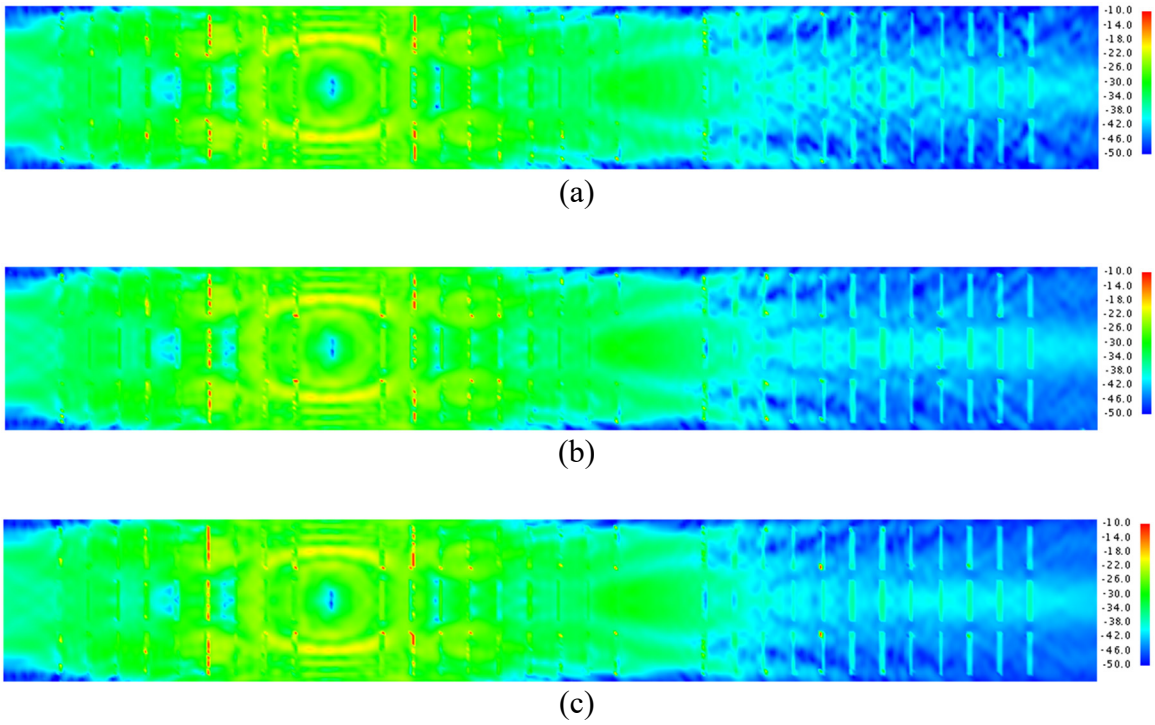

Fig. 6. Typical color plots of Poynting vector magnitude for fifth-scale model simulations demonstrating better convergence of the fifth-scale simulations relative to the full-scale simulations with ray-tracing angular increments of (a) 0.7 degrees, (b) 0.5 degrees, and (c) 0.3 degrees.

with distance particularly in areas of low Poynting vector magnitudes near the front and back of the plane for the full-scale plane model not nearly as present in the smoother plots of the fifth-scale model. This spottiness is attributed to the poorer convergence of the larger model, although the full-scale model convergence is still acceptable given the spottiness occurs primarily for low signal strengths. Second, the results of the full-scale model exhibit reduced Poynting vector magnitudes (a reduction of about 15 dB or a linear-scale factor of about 25 times) relative to the scaled-down model as would be expected given the fifth-scale model concentrates the transmitted power in a smaller space. Scaling down the model by a factor of five decreases model areas by a factor of twenty-five and therefore an increase by a linear-scale factor of twenty-five in the

Poynting vector magnitudes of the scaled-down model would be anticipated. A linear-scale factor will only add a constant value to the decibel-scale Poynting vector magnitude and therefore not be expected to affect the slope (path loss factor) and variability (standard deviation of shadowing) of the linear regression of decibel-scale Poynting vector magnitude against logarithmic distance. Overall, the convergence tests show good qualitative agreement with similar dynamic ranges between the models and with correlation between the model results showing the majority of signal power being concentrated in rings near the transmitter with the signal strength exhibiting large-scale attenuation with TX-RX separation. The use of the fifth-scale model for simulating the path loss parameters is therefore reasonable. Estimates of the path loss model parameters for both the full-scale model and for the fifth-scale model are included in Results for comparison.

With the convergence of the simulation results having been demonstrated, we will move into an overview of the results of the simulations. Regression estimates of the path loss factor and standard deviation of shadowing based on the simulated Poynting vector magnitudes were made for eight regression scenarios. Simulations of both full-scale and fifth-scale plane models were computed with and without passengers seated in all chairs. For the results of each of these four simulations, regressions were computed for the in-flight (from back to front) and in-rear directions of signal propagation relative to the transmitter for the nine paths parallel to the y-axis of the coordinate system (along the length of the fuselage) as mentioned previously and shown in Fig. 4 above. A summary

of these simulation scenarios with their respective identification numbers is given in Table III.

TABLE III
Summary of Simulation Scenarios

Scenario Number	Model Scale	Seating	Direction
1	1	Empty	In-flight
2	1	Empty	In-rear
3	1	Filled	In-flight
4	1	Filled	In-rear
5	0.2	Empty	In-flight
6	0.2	Empty	In-rear
7	0.2	Filled	In-flight
8	0.2	Filled	In-rear

These simulation scenarios and regression paths provide a test of the effects on the simulated path loss parameters of scaling the plane model, of the presence of lossy passengers, of the direction of propagation, and of the lateral (x-coordinate) receiver position within the plane. Prior to the simulations it was predicted that greater loss path factors and greater standard deviations of shadowing would be estimated for paths with greater obstruction and more complexity as signal obstruction tends to block signals and to increase signal attenuation. Paths further from the centerline of the plane (i.e. having greater absolute x-coordinate values) with less direct paths between the transmitter and the receiver positions would then be predicted to have greater values for these parameters as would models with lossy passengers in comparison to empty models. The resulting estimates of path loss factor and standard deviation of shadowing computed from the

simulations agree with some of these assumptions and partially with the above mentioned values obtained empirically by other authors as discussed in the next chapter. The simulation estimates show great promise for the use of ray-tracing simulations of signal strength for predicting the large-scale fading path loss parameters of path loss factor and standard deviation of shadowing with additional model development.

CHAPTER THREE

Results

The path loss parameters estimated from the simulations are in line with the empirical results of other authors and with many of the qualitative predictions discussed previously. In Fig. 7, plots of the simulated Poynting vector magnitude versus TX-RX distance and the resulting regression lines are shown for scenario 6 for the nine regression paths along the length of the aircraft cabin. These plots are typical for all of the simulation scenarios with a log-linear relationship between decibel-scale Poynting vector magnitude and distance being clearly present. Additionally, large-scale shadowing variability and small-scale fading in the signal strength (high variability in signal strength over short distances due to multipath interference), a key feature observed in real measurements of signal strength, can be seen in the plots. However in some of the plots, increases in Poynting vector magnitude of over 10 dB over short changes in distance are observed. These increases are significantly greater than what would be statistically expected to be caused by multipath interference or shadowing and potentially indicate poor convergence in some locations along the receiver plane. The spikes however occur over short distance intervals and should not significantly affect the final regression values. The results also show strong symmetry between plots for the regression paths on opposite sides of the cabin (i.e. with the same absolute value of x-coordinate value) as would be expected given the symmetry of the plane model and given the transmitter position being along the centerline of the plane at the x-coordinate value of zero.

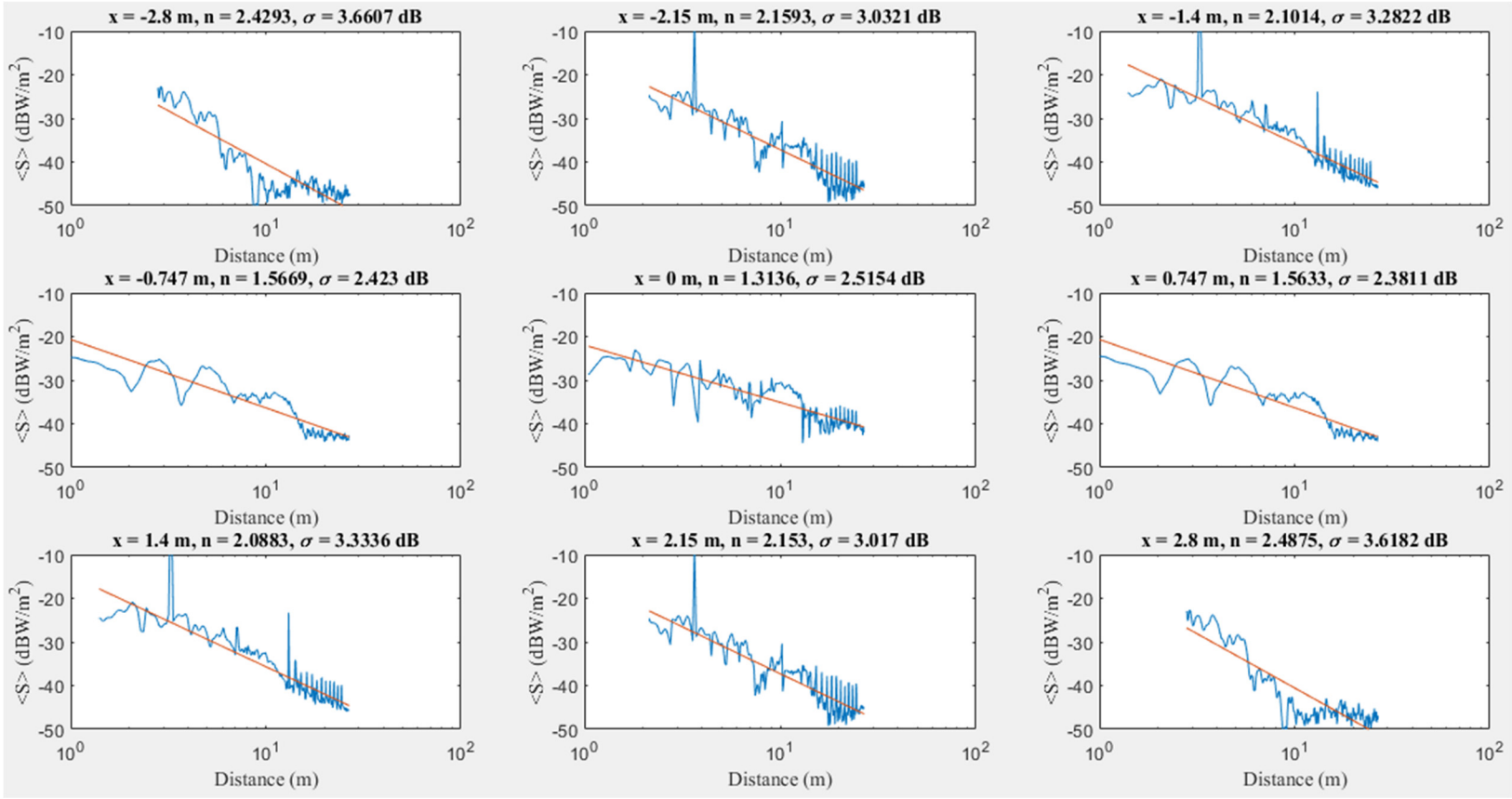

Fig. 7. Plots of Poynting vector magnitude versus logarithmic TX-RX distance for the nine regression paths of simulation scenario 6 (a typical plot for all of the simulation scenarios).

In Tables IV and V, regression estimates of path loss factor and standard deviation of shadowing are given respectively for the cabin regression paths of each simulation scenario. In Figures 8 and 9, path loss factor and standard deviation of shadowing are plotted respectively against x-coordinate of regression path for each simulation scenario. In these tables and plots, only the values for the regressions of one side of the plane are shown due to the strong symmetry of the results across the left and right side of the plane eliminating the need to give values for all of the regression paths.

Table IV
Simulated Path Loss Factors

	Scenario Number	Simulated Path Loss Factor, n					
x-Coordinate of Regression (m)		0	0.747	1.4	2.147	2.8	Average
	1	0.97	0.37	1.19	1.75	2.07	1.27
	2	0.90	0.78	1.91	1.40	1.26	1.25
	3	1.15	0.42	1.31	1.41	1.83	1.22
	4	1.05	0.85	1.95	1.38	0.92	1.23
	5	1.03	0.94	1.29	1.79	3.94	1.80
	6	1.31	1.56	2.09	2.15	2.49	1.92
	7	0.27	0.76	1.45	2.29	3.36	1.63
	8	1.64	1.49	1.92	2.04	1.96	1.81

TABLE V
Simulated Standard Deviations of Shadowing

	Scenario Number	Simulated Standard Deviation of Shadowing, σ (dB)					
x-Coordinate of Regression (m)		0	0.747	1.4	2.147	2.8	Average
	1	3.26	3.24	1.93	2.89	3.01	2.87
	2	3.44	2.60	2.71	2.89	3.39	3.01
	3	3.36	3.26	1.58	2.63	3.22	2.81
	4	3.84	2.86	2.82	2.85	3.88	3.25
	5	2.69	2.14	2.92	5.05	2.46	3.05
	6	2.52	2.38	3.33	3.02	3.62	2.97
	7	2.98	2.05	3.06	6.72	2.51	3.46
	8	3.64	2.10	3.50	3.45	3.20	3.18

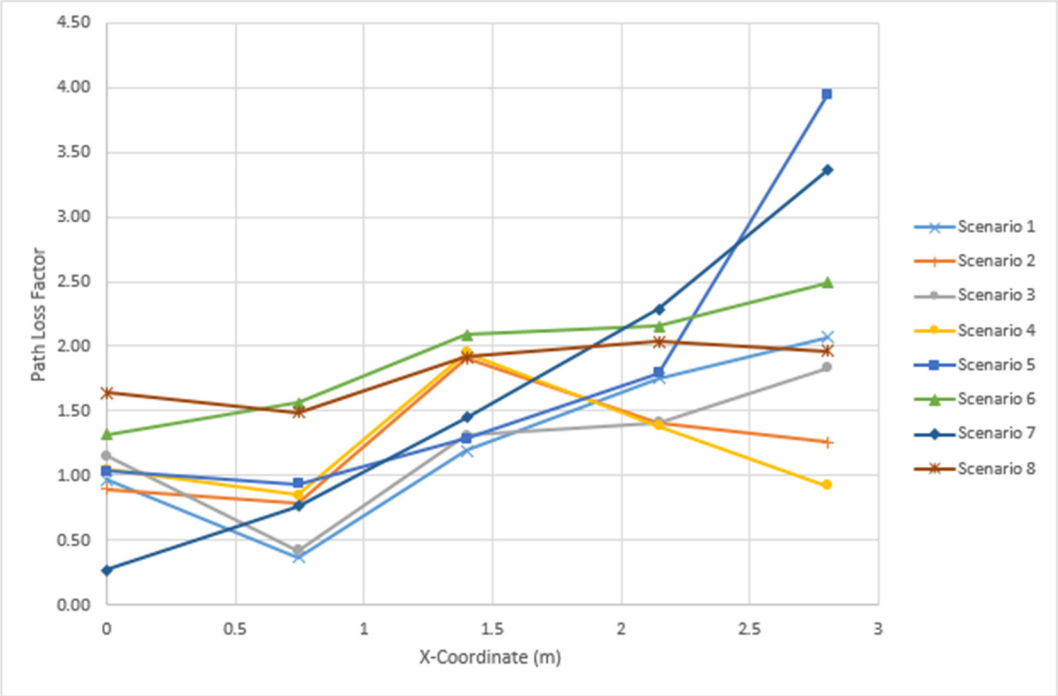

Fig. 8. Path loss factor vs. x-coordinate of regression path for all simulation scenarios.

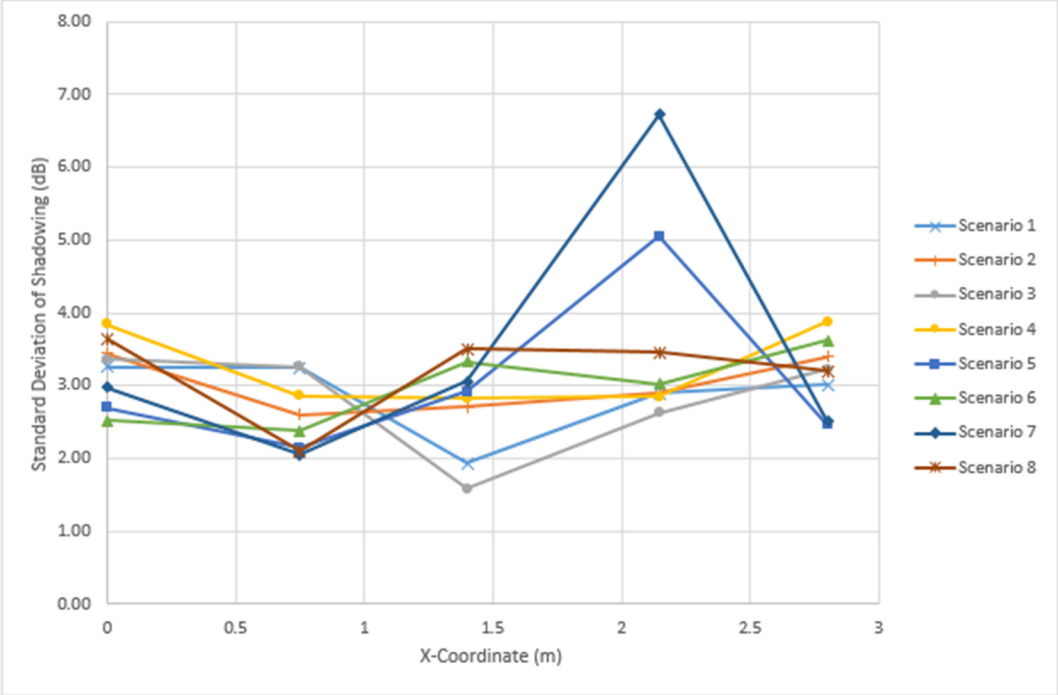

Fig. 9. Standard deviation of shadowing vs. x-coordinate of regression path for all simulation scenarios.

The simulated path loss parameters and standard deviations of shadowing generally agree with the empirical values of the authors mentioned above and many of the discrepancies between the measured and simulated values can be plausibly explained by the choice of plane model used. With the exceptions of scenarios 5 and 7 for 2.8 m, the simulated path loss factors fall within the range of factors from 0.2 to 2.7 found empirically by other authors. Examining these path loss factors further, we see a general increase in the path loss factor with x-coordinate value of the regression paths with all path loss factors being greater at 2.8 m than at 0 m and with monotonic or nearly monotonic increases with x-coordinate value of regression path being observed for all simulation scenarios but 2 and 4. This trend is in line with the prediction of increased path loss factor for regression paths further from the centerline of the plane cabin based on an expected increase in clutter and signal obstruction for paths further from the centerline of the plane.

The simulated path loss factors are generally lower than what might be predicted from the measured values for similar measurement scenarios by other authors with most of the simulated factors being well below the free space path loss factor of two and with an average path loss factor of 1.52 across all scenarios and regression paths even while the regression paths for all of the simulation scenarios would be considered NLOS signal propagation paths (with path loss factors above the free space value expected from the measured values of other authors). Of all the scenarios of the measurement campaigns of the authors mentioned above, the most directly comparable with the scenarios of these simulations are the NLOS scenarios of [3] which were conducted at 2.45 GHz along the

seats of the cabin of a smaller passenger plane with only 70 passengers seats. These measurement scenarios most closely match the conditions of the simulations and resulted in measured path loss factors of 2.2 and 2.7, values significantly higher than the general values predicted by the simulations. Strong waveguide effects are then exhibited in the simulations. It is possible the PEC shell of the plane model in combination with the sparsely furnished cabin area with lower amounts of lossy materials than found in real cabins led to significantly higher overall reflectivity in the plane fuselage. This theory would be supported by the low measured path loss factors between 0.20 and 2.08 (with the majority of measured path loss factors being below 1.5) found for the military plane studied in [8] with more metallic surfaces than typically found in commercial planes. The PEC shell of the simulation model is likely contributing too much reflectivity to the model and the limited lossy furnishings are likely not attenuating the signal enough. The simulated cabin is also far simpler than that of a real cabin, leading to reduced obstruction and signal dispersion and therefore likely contributing to the reduced attenuation. A more accurate model of a real commercial cabin reasonably could reduce these discrepancies.

The standard deviations of shadowing with an average value of 3.07 dB and a range from 1.58 dB to 6.72 dB also agree with most of the measured deviations with a tendency toward being lower than the measured values. For the measurement scenarios of [3] most directly comparable to the simulations, standard deviations of shadowing of 8 dB and 9.8 dB were obtained, both of which are higher than all of the simulated deviations. These discrepancies in standard deviation of shadowing between the simulated and measured values can also be explained by the greatly reduced complexity

of the simulation model relative to the complexity of real planes with the simulation model having enlarged, simplified features having little detail or variety with the passengers and chairs being respectively identical and composed of primitive cuboids. Lower complexity would produce lower signal scattering and therefore lower variation in signal strength and lower standard deviations of shadowing. The deviations across the scenarios also appear to remain generally constant with regression x-coordinate (with some variation occurring between the two variables with no clear relation) with the deviations of the regression paths at 0 m being close to those at 2.8 m. This finding does not agree with the prediction of increased deviations for the less direct paths further from the centerline of the cabin model however this effect could also due in part to the reduced complexity and accuracy of the model.

The effects of scaling the simulation model are unexpected. Comparing the path loss factors and standard deviations of shadowing respectively averaged across all regression paths between the corresponding pairs of full-scale and fifth-scale simulation scenarios of scenario 1 (n = 1.27, $\boldsymbol{\sigma}$ = 2.87 dB) versus scenario 5 (1.8, 3.05 dB), 2 (1.25, 3.01 dB) versus 6 (1.92, 2.97 dB), 3 (1.22, 2.81 dB) versus 7 (1.63, 3.46 dB), and 4 (1.23, 3.25 dB) versus 8 (1.81, 3.18 dB), clear trends may be seen. The average path loss factors of the full-scale simulations with an average of 1.24 show little variance and are significantly lower than those of the fifth-scale simulations which have greater (but still low) variance and an average of 1.79. This finding of significant difference between the path loss factors of the scaled and unscaled models (whereas the factors would agree if the scaled simulations were an accurate representation of the full-scale model) may be

due to the reduced convergence and therefore accuracy of the full-scale model relative to the fifth-scale model (particularly since the fifth-scale model path loss factors are larger and more closely match the empirical factors). However more simulation (starting with more accurate simulation of the full-scale model) is required to validate this hypothesis and the assumption that scaling down the model is a legitimate means of reducing computational complexity of simulation. The standard deviations of path loss on the other hand match much more closely between the full-scale and fifth-scale simulations with averages of 2.98 dB and 3.17 dB respectively, providing some evidence of the accuracy of the results of the scaled model.

The simulation effects of passengers are also interesting. Similarly we compare the factors and deviations respectively averaged across all regression paths between the corresponding pairs of empty and passenger-filled simulation scenarios of scenario 1 (1.27, 2.87 dB) versus scenario 3 (1.22, 2.81 dB), 2 (1.25, 3.01 dB) versus 4 (1.23, 3.25 dB), 5 (1.8, 3.05 dB) versus 7 (1.63, 3.46 dB), and 6 (1.92, 2.97 dB) versus 8 (1.81, 3.18 dB). The average path loss factors of the simulations of empty cabins have an average of 1.56 and tend to be slightly greater than those of the simulations of seated cabins with an average of 1.47 (but with a smaller difference than the difference between path loss factors of the full-scale and fifth-scale models). This result shows the passengers used in these simulations slightly decrease the simulated path loss factor instead of increasing the factor as predicted from the assumption that the passenger bodies would represent additional signal obstruction (as the results of [4] indicate as discussed above), suggesting the passenger bodies should be made lossier and more complex and experimented with in

future simulations to increase the accuracy of the simulations. The average standard deviations of path loss for the simulations of empty cabins with an average of 2.98 dB are generally slightly lower than those of the filled cabin with an average 3.18 dB. This finding is more in line with the prediction that the passengers increase the obstruction and complexity of the cabin for signal propagation.

Finally discussing the last varied dimension of the simulations, the effects of propagation direction are the most in line with our predictions. Comparing the factors and deviations respectively averaged across all regression paths between the corresponding pairs of scenarios with in-flight and in-rear propagation directions respectively of scenario 1 (1.27, 2.87 dB) versus 2 (1.25, 3.01 dB), 3 (1.22, 2.81 dB) versus 4 (1.23, 3.25 dB), scenario 5 (1.8, 3.05 dB) versus 6 (1.92, 2.97 dB), and 7 (1.63, 3.46 dB) versus 8 (1.81, 3.18 dB), an agreement may be seen between the parameters of the two signal propagation directions. The average path loss factors for the simulation scenarios of the in-flight propagation direction have an average of 1.48 and those for the simulation scenarios of in-rear propagation direction have an average of 1.55. Given the fact that the chairs used in the simulation model use identical materials for the front and backs of the seats and given the fact that the cabin is similar structurally in the two propagation directions, this agreement between the factors of the two directions is reasonable and in line with the work of [5]. The average standard deviations of path loss for the simulation scenarios of the in-flight propagation direction with an average of 3.05 dB also match those for the in-rear propagation direction with an average of 3.10 dB. Again, this finding

further corroborates the similarity between the simulated propagation between the in-flight and in-rear propagation directions.

The simulated path loss factors and standard deviations of shadowing generally agree with and fall within the range of the empirical values of other authors with a tendency toward being lower than the measured values. While the simulation model may need additional tuning to increase the accuracy, specifically in terms of increasing model attenuation and shadowing effects as well as the (ideally) attenuating effects of the passenger bodies, and to validate the choice of model scaling, the ray-tracing method, specifically the FEKO RL-GO EM solver, coupled with a simplified cabin CAD model shows promise for efficiently estimating the path loss factors and standard deviations of shadowing in an aircraft cabin environment.

CHAPTER FOUR

Conclusions

Simulations of signal propagation will become increasingly necessary as consumer demand for wireless connectivity on planes continues to rise. This paper explored the use of a ray-tracing algorithm, the FEKO RL-GO solver, to simulate two large-scale fading parameters, the path loss factor and the standard deviation of shadowing, both of which are significant for determining wireless coverage area. The resulting simulated path loss parameters are in good agreement with the measured values of several other authors. The simulated path loss factors generally increase as the regression path moves away from the center of the plane toward more indirect paths near the sides of the plane as expected. These simulated parameters however trend toward being lower than the measured values and do not exhibit several of the expected qualitative relations predicted with regard to the simulation model scale or the level of passenger filling.

To address these problems, the model accuracy may be improved in a number of ways. First, the CAD model could be made to more faithfully represent the structure of real planes with the inclusion of the structures of an aisle, a cockpit, a crew area in the rear of the plane, an overhead compartment, and dielectric cabin side walls. Adding more lossy, complex signal obstructions typically present in plane cabins would tend to increase the attenuation and variance of the signal strength, raising both of the model parameters into ranges in closer agreement with empirical results. More experimentation

is needed to determine the reason why the passenger bodies did not increase signal attenuation as predicted and to find the best method for simply modeling human passengers more accurately. Generally a method for quantitatively characterizing the degree of model fidelity or model resolution for ray-tracing methods must be developed, possibly with parameters such as minimum and average component dimension compared between the model and the modeled environment, and additionally the model must be modeled after a specific plane rather than after generic plane structures common to all planes. Most notably the technique of scaling down the plane model dimensions to increase the convergence of the model and to reduce the computational complexity of the simulations must be further explored as this assumption was clearly challenged by the results of these simulations. The convergence of the simulations must also be improved as indicated by the large, rapid increases in Poynting vector magnitude of over 10 dB present in the simulation results. Many additional parameters could also be explored for this plane model. The transmitter could be moved throughout the cabin and the elevation of the receiver plane could be changed. More levels of passenger filling could be simulated. Varying more parameters could provide other sources of information for improving the model.

The results of the ray-tracing simulations agree well enough with the parameters predicted from empirical results to demonstrate the potential of the method to simulate the large-scale path loss parameters of path loss factor and standard deviation of shadowing with simplified plane models. The utility of the ray-tracing solver is clear and further work is needed to optimize and validate the method.

REFERENCES

[1] A. Jahn *et al*., "Evolution of aeronautical communications for personal and multimedia services," in *IEEE Communications Magazine*, vol. 41, no. 7, pp. 36-43, July 2003. doi: 10.1109/MCOM.2003.1215637

[2] C. Metz, "IP-over-Satellite:Internet Connectivity Blasts Off," IEEE Internet Comput., vol. 4, (4), pp. 84-89, 2000. Available: http://ezproxy.baylor.edu/login?url=https://search.proquest.com/docview/197333868?accountid=7014. DOI: http://dx.doi.org/10.1109/4236.865091.

[3] H. Saghir, C. Nerguizian, J. J. Laurin and F. Moupfouma, "In-Cabin Wideband Channel Characterization for WAIC Systems," in *IEEE Transactions on Aerospace and Electronic Systems*, vol. 50, no. 1, pp. 516-529, January 2014. doi: 10.1109/TAES.2013.120089

[4] J. Chuang, N. Xin, H. Huang, S. Chiu and D. G. Michelson, "UWB Radiowave Propagation within the Passenger Cabin of a Boeing 737-200 Aircraft," 2007 IEEE 65th Vehicular Technology Conference - VTC2007-Spring, Dublin, 2007, pp. 496-500. doi: 10.1109/VETECS.2007.113

[5] T. Cogalan, S. Videv and H. Haas, "Aircraft In-Cabin Radio Channel Characterization: From Measurement to Model," *GLOBECOM 2017 - 2017 IEEE Global Communications Conference*, Singapore, 2017, pp. 1-6. doi: 10.1109/GLOCOM.2017.8254554

[6] Rappaport, Theodore S. Wireless Communications Principles and Practice, Second Edition. Prentice Hall, 2002.

[7] A. Skrebtsov, A. Burnic, Dong Xu, A. Waadt and P. Jung, "UWB applications in public transport," 2011 International Conference on Communications, Computing and Control Applications (CCCA), Hammamet, 2011, pp. 1-4. doi: 10.1109/CCCA.2011.6031519

[8] C. G. Spiliotopoulos and A. G. Kanatas, "Path-Loss and Time-Dispersion Parameters of UWB Signals in a Military Airplane," in IEEE Antennas and Wireless Propagation Letters, vol. 8, pp. 790-793, 2009.

[9] B. Xu, F. Zhang, L. Dong and Y. Li, “Wideband propagation channel

measurement in a hallway environment," IEEE MTT 2014 Texas Symposium on Microwave and Wireless Circuits and Systems, Waco, TX, Apr. 2014.

[10] C. De Raffaele, C. J. Debono and A. Muscat, "Modeling electromagnetic interference generated by a WLAN system onboard commercial aircraft," Melecon 2010 - 2010 15th IEEE Mediterranean Electrotechnical Conference, Valletta, 2010, pp. 699-704. doi: 10.1109/MELCON.2010.5475991

[11] K. Chetcuti, C. J. Debono, R. A. Farrugia and S. Bruillot, "Wireless propagation modelling inside a business jet," IEEE EUROCON 2009, St.-Petersburg, 2009, pp. 1644-1649. doi: 10.1109/EURCON.2009.5167863

[12] M. C. Lawton and J. P. McGeehan, "The application of GTD and ray launching techniques to channel modelling for cordless radio systems," *[1992 Proceedings] Vehicular Technology Society 42nd VTS Conference - Frontiers of Technology*, Denver, CO, 1992, pp. 125-130 vol.1. doi: 10.1109/VETEC.1992.245457

[13] J. Peatross and M. Ware, Physics of Light and Optics, 2015 ed. Salt Lake City, UT, 2017. Available: http://optics.byu.edu/BYUOpticsBook_2015.pdf

[14] E. Shamonina, V. A. Kalinin, K. H. Ringhofer and L. Solymar, "Short dipole as a receiver: effective aperture shapes and streamlines of the Poynting vector," in IEE Proceedings - Microwaves, Antennas and Propagation, vol. 149, no. 3, pp. 153-159, Jun 2002.

[15] A. G. Aguilar, J. van Tonder, U. Jakobus and F. Illenseer, "Overview of recent advances in the electromagnetic field solver FEKO," 2015 9th European Conference on Antennas and Propagation (EuCAP), Lisbon, 2015, pp. 1-5.